Mon. Not. R. Astron. Soc. **000**, 1–11 (2004) Printed 2 February 2008 (MN LATEX style file v2.2)

# X-ray properties of UV-selected star forming galaxies at $z \sim 1$ in the Hubble Deep Field North

E. S. Laird,[1⋆] K. Nandra,[1] K. L. Adelberger,[2] C. C. Steidel,[3] N. A. Reddy[3]
[1] *Astrophysics Group, Imperial College London, Blackett Laboratory, Prince Consort Road, London SW7 2AZ, UK*
[2] *Carnegie Observatories, 813 Santa Barbara Street, Pasadena, CA 91101, USA*
[3] *California Institute of Technolgy, MS 105-24, Pasadena, CA 91125, USA*

arXiv:astro-ph/0501411v1 19 Jan 2005

Accepted January 2005.

**ABSTRACT**

We present an analysis of the X-ray emission from a large sample of ultraviolet (UV) selected, star forming galaxies with $0.74 < z < 1.32$ in the *Hubble Deep Field* North (HDF-N) region. By excluding all sources with significant detected X-ray emission in the 2 Ms *Chandra* observation we are able to examine the properties of galaxies for which the dominant emission in both UV and X-ray is expected to be predominantly due to star formation. Stacking the X-ray flux from 216 galaxies in the soft and hard bands produces significant detections ($14.9\sigma$ and $3.2\sigma$, respectively). The derived mean 2–10 keV rest-frame luminosity is $2.97 \pm 0.26 \times 10^{40}$ erg s$^{-1}$, corresponding to an X-ray derived star formation rate (SFR) of $6.0 \pm 0.6$ M$_\odot$ yr$^{-1}$. Comparing the X-ray value with the mean UV derived SFR, uncorrected for attenuation, we find that the average UV attenuation correction factor is $\sim$3. By binning the galaxy sample according to UV magnitude and colour, and stacking the observed frame soft band X-ray flux in each bin, correlations between UV and X-ray emission are examined. We find a strong positive correlation between X-ray emission and rest-frame UV emission, consistent with a strict linear relationship, $L_X \propto L_{UV}$, at the 90 per cent level. A correlation between the ratio of X-ray-to-UV emission and UV colour is also seen, such that $L_X/L_{UV}$ increases for redder galaxies. We find no direct relation between X-ray flux and UV colour. Given that X-ray emission offers a view of star formation regions that is relatively unaffected by extinction, results such as these can be used to evaluate the effects of dust on the UV emission from high-$z$ galaxies. For instance, using the observed correlation between UV colour excess and the ratio of X-ray-to-UV emission – a measure of UV obscuration – we derive a relationship for estimating UV attenuation corrections as a function of colour excess. The observed relation is inconsistent with the Calzetti et al. (2000) reddening law which over predicts the range in UV attenuation corrections by a factor of $\sim$100 for the UV selected $z\sim1$ galaxies in this sample.

**Key words:** galaxies: starburst – galaxies: high-redshift – X-rays: galaxies

## 1 INTRODUCTION

The vast majority of known high redshift galaxies are selected in the rest-frame ultraviolet (UV). For instance the Lyman break technique, which selects actively star forming galaxies based on their broad band ultraviolet (UV) colours, is the primary method for efficiently selecting redshift $z \gtrsim 3$ galaxies (e.g. Steidel et al. 1996; Steidel et al. 1999; Steidel et al. 2003) and has inspired similar techniques to isolate star forming galaxies from $1 \lesssim z \lesssim 3$ (Adelberger et al. 2004; Steidel et al. 2004). The galaxies identified in these surveys are observed during the peak of the cosmic star formation rate density (e.g Lilly et al. 1996; Madau et al. 1996; Hughes et al. 1998) and represent a significant fraction of the total star formation at high redshift (Adelberger & Steidel 2000). The star formation rates (SFRs) derived from these UV-selected galaxies are therefore crucial for determining the history of star formation and heavy element production in the Universe.

However the SFRs obtained from the rest-frame UV fluxes are very sensitive to the effects of dust attenuation intrinsic to the galaxies (Kennicutt 1998). Correcting the observed fluxes for the attenuation requires an understanding about the true nature of the

⋆ E-mail: e.laird@imperial.ac.uk;

sources and their dust content that is currently lacking. To overcome this, average corrections are applied based on dust attenuation laws observed in local starburst galaxies (e.g. Calzetti, Kinney, & Storchi-Bergmann 1994; Calzetti et al. 2000; Meurer, Heckman, & Calzetti 1999, hereafter MHC99), which appear to be the local analogues of the high redshift LBGs (e.g. Steidel et al. 1996; Giavalisco 2002). However there is considerable disagreement about the size of the corrections to be applied with some evidence that attenuation has been overestimated (Bell 2002).

X-ray observations can add to this debate by providing a view of galaxies that is relatively unaffected by dust and extinction. Hard X-rays are emitted from star forming galaxies by a combination of high mass X-ray binaries (HMXBs), supernovae remnants and hot gas (Fabbiano 1989). Locally strong correlations between X-ray luminosity and other SFR measures have been seen (David, Jones, & Forman 1992), showing that X-ray luminosity can be used as a SFR measure (Ranalli, Comastri, & Setti 2003; Grimm, Gilfanov, & Sunyaev 2003; Nandra et al. 2002). By comparing X-ray derived SFRs with UV estimates we can independently check the validity of the attenuation corrections and gain insight into the nature and dust content of the UV-selected galaxies in the early Universe.

Although the majority of high redshift star forming galaxies are not bright enough to be detected with the current class of X-ray telescopes, with deep *Chandra* observations the average properties of a sample can be determined using stacking techniques (e.g. Hornschemeier et al. 2001; Brandt et al. 2001; Nandra et al. 2002). Several efforts at this have already been made. Brandt et al. (2001) stacked the emission from 24 $z\sim3$ LBGs in the 1 Ms Chandra Deep Field-North (CDF-N), detecting a significant 0.5–2 keV observed-frame signal. Using local starburst reddening relations Seibert, Heckman, & Meurer (2002) predicted the mean X-ray luminosity of the 24 LBGs and found it agreed well with the stacking results. Also in the 1 Ms CDF-N, Nandra et al. (2002) analysed the emission from two much larger samples of 148 $z\sim3$ LBGs and 95 $z\sim1$ star forming galaxies. More recently using the 2 Ms data in the GOODS-North field, Reddy & Steidel (2004) analysed the stacked emission from a sample of UV-selected $z\sim2$ galaxies and **?** analysed the emission from large samples of $z\simeq3$, 4, 5 and 6 LBGs.

In this paper we seek to add to this work by improving upon and extending the analysis of the $z\sim1$ galaxies by Nandra et al. (2002; hereafter N02) using the 2 Ms observation of the HDF-N region. Using a much larger catalogue of 255 $z\sim1$ UV-selected Balmer break galaxies (BBGs) we assess the X-ray properties and the relations between UV and X-ray emission of the galaxies, during a period where the star formation density of the Universe was at its peak. Throughout, we assume a standard, flat ΛCDM cosmology with $\Omega_\Lambda = 0.7$ and $\mathrm{H}_0 = 70$ km s$^{-1}$ Mpc$^{-1}$.

## 2 DATA AND ANALYSIS

### 2.1 Optical data

The BBG candidates were colour selected from optical images using photometric criteria, detailed in Adelberger et al. (2004). Briefly, the BBGs have been selected based on the strengths of the Balmer and 4000 Å breaks in their spectral energy distributions, designed to identify starburst, Sb- and Sc-type star forming galaxies (Adelberger et al. 2004). The candidate list, which includes all BBGs with spectroscopically confirmed redshifts with $0.74 < z < 1.32$, is considerably larger than that used in N02 thanks to the extensive spectroscopic effort of the Team Keck Treasury Redshift Survey in the Great Observatories Origins Deep Survey (GOODS)-North field (Wirth et al. 2004). There are 255 galaxies in our CDF-N BBG sample, with $\overline{z}$=0.95. $U_n, G, \mathscr{R}$ and $I$ magnitudes and colours have been measured for all the objects.

### 2.2 X-ray data

The HDF-N region has been observed with *Chandra* ACIS-I 20 times since launch, with the total exposure time approximately 2 Ms. Analysis of these observations, and a point source catalogue, was presented in Alexander et al. (2003; hereafter A03). For this paper we used the raw data available from the public archive.

The HDF-N was observed over a period of 27 months during which time the observing conditions and operating mode of the telescope changed. The 20 observations can broadly be separated into three groups: the first three observations were taken in Faint mode with a focal plane temperature of $-110^\circ$C, the following 9 observations also in Faint mode with temperature $-120^\circ$C, and the final 8 observations, constituting the second 1 Ms, taken in Very Faint mode at -120° C. The differences in the observing modes at times warranted separate treatment when reducing the data.

Our analysis is restricted to an approximately $10\farcm3 \times 10\farcm3$ region within the larger ACIS-I field of view. This encompasses the optical BBG survey region ($8\farcm7 \times 8\farcm7$).

### 2.3 Data reduction

Data reduction was carried out using the *Chandra* X-ray Center (CXC) *Chandra* Interactive Analysis of Observations (CIAO) software, version 3.0.1, and the *Chandra* calibration database (CALDB) version 2.23. Using the tool ACIS_PROCESS_EVENTS, all observations had up-to-date gain maps and geometry solutions applied. In addition, the observations taken at -120° C were corrected for radiation damage inflicted in the first few months of *Chandra* operations using the standard CXC CTI correction, and the eight observations taken in Very Faint mode were further cleaned by identifying likely background events. The event files were filtered using standard screening criteria – ASCA event grades 0,2,3,4,6, Good Time Intervals and status=0 – to remove bad and flaring pixels, bad columns, cosmic ray afterglows etc. Source subtracted lightcurves were created and periods where the background was more than $3\sigma$ from the mean value were flagged using ANALYZE_LTCRV. All the periods of high background identified by ANALYZE_LTCRV were removed in addition to a further 44.4 ks from observation 2344 where the procedure failed to identify a flare and 15.2 ks from observation 3389 where it failed to identify the full duration of a flare.

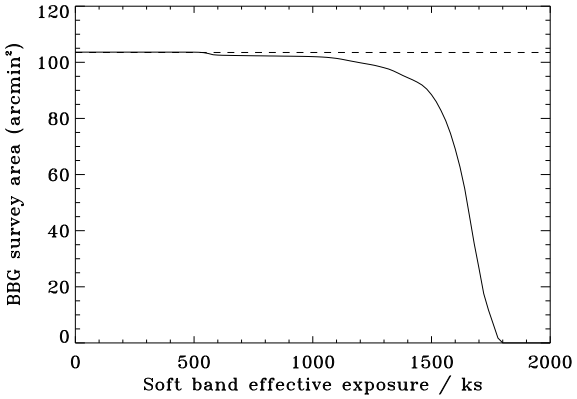


**Figure 1.** The BBG survey area versus the minimum effective exposure in the soft-band exposure map. The dashed line shows the solid angle of the region of our analysis. Over 98 per cent of the BBG area has at least 1 Ms effective exposure and over 85 per cent has at least 1.5 Ms.

Before coadding the event files, the relative astrometry was improved by registering each observation to the coordinate frame of observation 1671 using bright sources within 6 arcminutes of the aim points. This was done using the ALIGN_EVT tool written by T. Aldcroft[1]. The root-mean-square shift applied to the observations was 0.54 arcseconds in RA and 0.38 arcseconds in Dec. The average aim point for the combined observations, weighted by exposure time, was $\alpha = 12^{\rm h}36^{\rm m}47\overset{\rm s}{.}59$, $\delta = +62^\circ14'08\overset{''}{.}1$ (J2000.0) and the total exposure time was 1.86 Ms.

We constructed event files and images in four bands: 0.5–2 keV (soft band), 0.5–7 keV (full band), 2–7 keV (hard band) and 4–7 keV (ultra-hard band). Effective exposure maps were constructed using the MERGE_ALL tool for each of the four bands – these take into account the effects of vignetting, gaps between chips, bad column and bad pixel filtering and are required for converting observed counts to flux. The maps were created at a single energy representative of the photons in each band: 1 keV for the soft, 2.5 keV for the full, 4 keV for the hard and 5.5 keV for the ultra-hard band. These are the mean photon energies of detected sources in the band. Given that bad pixel files for observations in different modes vary considerably, and that MERGE_ALL will only accept one bad pixel file, in order to properly account for their effect we created separate exposure maps for each of the three groups of observations described above. These maps were then re-gridded to produce effective exposure maps for the full ∼ 2Ms. A plot of solid angle over the BBG survey area as a function of soft band effective exposure is shown in Figure 1.

When performing photometry with *Chandra* images the energy-dependent and position-dependent point-spread function (PSF) must be properly accounted for. Due to the different aim points of the 20 observations in the HDF-N a given sky position will have a different PSF in each observation and the final PSF should therefore represent the average value. To calculate the PSF for a given sky position we used the MKPSF tool with the CALDB PSF library file acisi1998-11-052dpsf1N0002.fits to create an image of the PSF at the corresponding detector position in each of the observations and then combined the images, weighted by exposure, to create an average PSF image. A radial profile of the PSF image was then obtained by extracting counts from 30 concentric circles out to a maximum radius of 30 arcseconds. Assuming all counts are contained within the 30 arcsecond radius we then calculated by interpolation the radius at which, say, 90 per cent of the counts are enclosed (referred to as the 90 per cent encircled energy fraction, EEF) and also the fraction of counts enclosed within a given fixed radius, say, 1.5 arcseconds[2]. This method can be repeated for different energies, positions, EEFs and radii.

Finally, PSF-corrected count rates should be converted to flux. For this conversion we have assumed a power-law source spectrum with $\Gamma$=2 in the all bands and Galactic column density $N_H = 1.6 \times 10^{20}$ cm$^{-2}$ (Stark et al. 1992). When converting from counts to flux the full, hard and ultra-hard bands were extrapolated to the standard upper-limit of 10 keV.

It has been found that the *Chandra* ACIS quantum efficiency (QE) has been suffering continuous degradation since launch – most likely a result of the build-up of material on the ACIS detectors or optical blocking filers (Marshall et al. 2004) – which affects the spectral response of the detectors and, therefore, the counts to flux conversion. We have calculated the necessary corrections to the fluxes using the ACISABS model, version 1.1-2[3,4]. For Galactic column density and $\Gamma$=2 the soft, hard, full and ultra-hard fluxes should be increased by 14.7, 0.6, 11.5 and 0.1 per cent respectively. All fluxes quoted in this paper have been corrected for the QE degradation.

### 2.4 Source detection

Source detection was carried out in the field, the reasons for which are threefold: (1) identify BBG galaxies that are directly detected at 2 Ms, (2) use these objects to determine any overall offsets between the coordinate reference frames of the optical and X-ray images[5], and (3) identify all X-ray sources for exclusion from the stacking background calculations. Source detection was performed using our own procedure, which is detailed in Nandra et al. 2005. To identify X-ray sources for exclusion from the stacking background determination we set the false probability threshold to $10^{-6}$, a level for which 1 spurious source is expected per band in the

[1] See http://cxc.harvard.edu/cal/ASPECT/align_evt/ for details.

[2] The assumption that all counts will be contained within 30 arcseconds may not always be strictly valid, particularly at large off axis angles (OAAs) and at high energies. However at the moderate OAAs considered in this work ($\simeq$ 6 arcminutes) any error introduced is likely to be very minor.

[3] For more information on the ACIS QE degradation see http://cxc.harvard.edu/cal/Acis/Cal_prods/qeDeg/.

[4] To take into account the time dependence of the degradation we applied the ACISABS correction to the response files for each individual observation then combined to obtain the exposure-weighted average correction.

[5] In order to increase signal-to-noise ratio any offset between coordinate reference frames should be corrected for before performing stacking analysis.

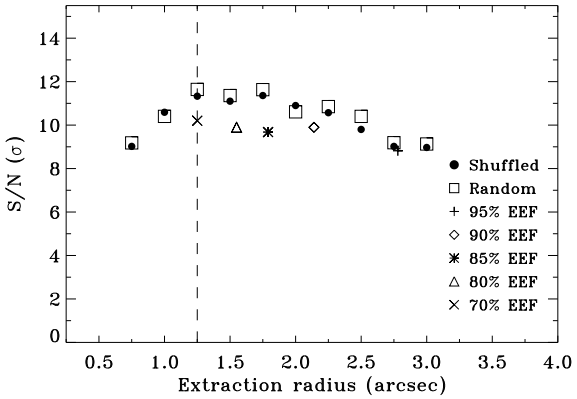


**Figure 2.** The signal-to-noise ratio vs. extraction radius in arcseconds. The signal-to-noise ratio is an inverse measure of the fractional error on the flux and is given by $(S/\sqrt{S+B})$, where S and B are the net source counts and background counts respectively. The two different background methods, shuffled and random positions, give very similar results. The results using a fixed fraction of the EEF are plotted at the average extraction radius used. The vertical dashed lines denote our chosen extraction radius of 1.25 arcseconds.

$10'.3 \times 10'.3$ survey area. To find only X-ray counterparts to the BBGs the threshold can be set much lower without introducing likely spurious X-ray sources as the area in question in considerably reduced. We used a threshold of $2 \times 10^{-4}$ which, given the number of BBGs and the area over which the BBG and *Chandra* catalogues are cross-correlated, results in a probability of a false X-ray detection of a BBG of less than 0.15 per cent per detection band. In each case sources were detected in the full, soft, hard and ultra-hard bands and a band merged catalogue produced.

The lower significance band merged *Chandra* catalogue was matched to the BBG catalogue to search for any X-ray counterparts and to identify any overall shift in the optical and X-ray reference frames that should be removed before performing stacking. A small overall offset between the two catalogues was found and the positions of the BBG candidates were shifted by -0.47 arcseconds in RA and -0.88 arcseconds in Dec to agree with the reference frame of the *Chandra* observation.

After correcting for this overall offset we re-matched the band merged *Chandra* catalogue to the BBG catalogue, using a radius of 1.5 arcseconds, to search for X-ray counterparts.

### 2.5 Stacking procedure

To determine the mean X-ray properties of the Balmer break galaxies that are too weak to be directly detected we employ a stacking technique similar to those described in N02 and Brandt et al. (2001).

We first identify all the candidates that have an X-ray counterpart and exclude them from the stacking. Secondly we identify any candidates with an unassociated, nearby X-ray source – these objects will be affected by the low-level PSF wings of the *Chandra* PSF and will lead to erroneously high source counts. We reject from the stacking all candidates which are separated from an X-ray source by a distance less than that of the 95 per cent EEF radius in that region. In a given stacking sample normally zero or one and never more than two sources were rejected. For the remaining galaxies in the samples we extract counts from the optical positions, summing both the detected counts and the number of pixels used for the extraction.

The background counts contributing to the total source signal are estimated in two ways. First we randomly shuffled the optical galaxy positions by 5–10 arcseconds and extracted counts from an X-ray source-masked image. Secondly we used random positions from anywhere over the $10'.3 \times 10'.3$ region of interest and again extracted counts from the masked image. In both cases, this was repeated 1000 times for each galaxy – sufficient to get an accurate estimate of the background counts and the dispersion. The counts and pixels were summed then scaled to the same area as the source extraction. Both background procedures produced very similar results – in this paper we quote all results for the shuffled positions, which should better account for any local variations in the background level.

The strength and accuracy of the observed signal is sensitive to the size of extraction radius used. A highly significant soft band detection of a smaller sample of BBGs in this field has already been achieved by N02: with the deeper data we therefore seek an extraction radius to minimize the flux errors rather than maximise the significance of the detection. We adopted an empirical approach to determining the optimal extraction radius – we tested 10 fixed extraction radii between 0.75 and 3.0 arcseconds, as well as the 70, 80, 85, 90 and 95 per cent EEF radii (Figure 2), selecting the option yielding the maximum signal-to-noise ratio. We chose a fixed extraction radius of 1.25 arcseconds[6], which gave a $14.9\sigma$ detection with a signal-to-noise ratio of 11.6 (we define detection significance as $S/\sqrt{B}$ and signal-to-noise ratio as $[S/\sqrt{S+B}]$, where S and B are the net source and background counts respectively). The appropriate PSF corrections for a 1.25 arcseconds extraction radius were calculated and the flux estimates corrected accordingly. We used the full sample of BBGs for the stacking and did not limit the analysis to sources at small off axis angles.

## 3 RESULTS

### 3.1 Directly detected sources

Of the 255 BBGs in our sample 37 are directly detected in X-ray. Some of these sources show clear evidence of harbouring an AGN (i.e. broad optical emission lines, X-ray luminosity greater than $10^{43}$ erg s$^{-1}$) while for others the X-ray emission could be due to an AGN, star formation, or a combination of both. In this paper we are concerned with the X-ray properties of galaxies where the emission is likely to be dominated by normal star forming processes and we consequently seek to omit from the analysis all galaxies where AGN emission may dominate. We therefore, conservatively, exclude all 37 of the directly detected galaxies and

[6] We note that N02 contains an error regarding the optimal extraction radius used. The paper states that the optimal radius found was 2.5 arcseconds – in fact 2.5 arcseconds was the optimal extraction diameter.

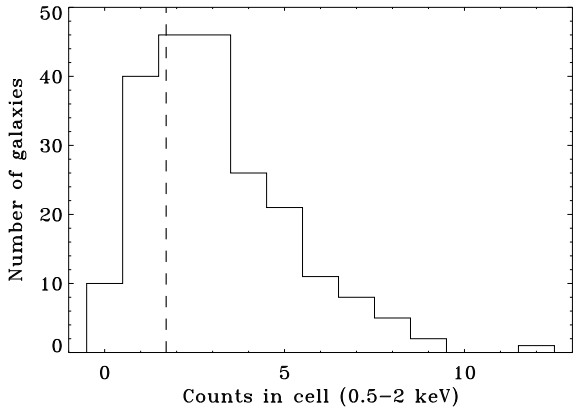


**Figure 3.** Count distribution for the undetected BBGs in the soft band. The vertical line denotes the mean background counts per count extraction cell, derived via the shuffle background method.

deal only with the undetected BBGs for the remainder of this paper. At $z\sim1$ this equates to removing all galaxies with $L_{2-10\ \rm keV} \gtrsim 10^{41}$ erg s$^{-1}$. Full analysis of the X-ray, optical and UV properties of the detected galaxies including starburst and AGN separation and identification will be addressed in an upcoming paper (Laird et al., in preparation).

### 3.2 Stacking results for undetected sources

Stacking the emission from the undetected BBGs produces significant detections in both the soft and hard bands (Table 1). In the soft band, stacking the counts from 216 undetected BBGs[7] produces a total of 290.8 net counts and a detection significance of 14.9. An average of 1.4 net counts per galaxy are detected, with 1.76 mean background counts in each galaxy extraction cell. The distribution of total counts (S+B) in an extraction cell (Figure 3) covers a wide range, with an almost continuous distribution of counts from the peak at 2–3 counts per cell up to ∼12 counts per cell and the realm of direct detections. Figure 3 demonstrates the stacking signal is not dominated by a few bright sources but instead well represents the entire sample. The detected soft band signal for the BBGs corresponds to a mean flux per galaxy of $5.51 \pm 0.49 \times 10^{-18}$ erg s$^{-1}$ cm$^{-2}$ (0.5–2 keV) and a mean luminosity of $L_{2-10\rm keV} = 2.97 \pm 0.26 \times 10^{40}$ erg s$^{-1}$. The mean flux per undetected BBG found here is in agreement with that found with the 1 Ms *Chandra* data for the smaller sample of BBGs by N02.

A low significance $3.2\sigma$ signal is detected from stacking the hard band emission from 216 undetected BBGs. There are 87.4 total net hard band counts detected, corresponding to an average of 0.40 net counts per galaxy. The expected background level is 3.4 mean counts per extraction cell. This weak but significant signal results in a mean 2–10 keV flux per BBG of $8.87 \pm 2.91 \times 10^{-18}$ erg s$^{-1}$ cm$^{-2}$. The spectral constraints implied by this detection are discussed in §4.1

[7] Two undetected BBGs are rejected from the stacking as described in §2.6

### 3.3 X-ray and UV correlations for stacked BBGs

The soft band signal for the undetected BBGs is strong enough to split the galaxy sample into subsets according to broad band properties and stack the X-ray emission for several bins, allowing the correlation of X-ray emission with observed-frame optical magnitudes and colours to be examined. In order to achieve reasonable signal-to-noise ratios, for each broad band property we split the sample into 6 bins based on $U_n, G, \mathscr{R}, I$ magnitude and $(U_n - G), (G - \mathscr{R}), (\mathscr{R} - I)$ colour. The range in redshift of the galaxies in our sample, $\Delta z \simeq 0.6$, means that a galaxies broad-band colour is not just a function of its intrinsic properties but is also a function of redshift. In order to investigate any correlations between UV colour and X-ray emission without a contaminating redshift effect we also calculate and bin according to the relative $(U_n - G), (G - \mathscr{R}), (\mathscr{R} - I)$ colour excess for the galaxies. For each colour $(U_n - G$ etc) the colour excess for each galaxy is calculated from the difference between the galaxy colour and the median colour of all galaxies with a redshift within $z = z \pm 0.05$ of the galaxy redshift. These values were binned and the mean colour excess for each bin was shifted so that the lowest value bin, which presumably contains the bluest and therefore least attenuated galaxies, was equal to zero. We denote this shifted colour excess by E(1800Å–2400Å), E(2400Å–3400Å) and E(3400Å–4050Å) for the $(U_n - G), (G - \mathscr{R})$ and $(\mathscr{R} - I)$ bands respectively, with the wavelengths denoting the approximate rest-frame wavelength of the emission in each filter. The stacking procedure used for the magnitude, colour and colour excess bins was identical to that carried out for the full samples of undetected sources.

The results of the subset stacking are shown in Figures 4 (binning according to magnitude) and 5 (binning on colour). For each quantity we show the exact mean 0.5–2 keV flux per galaxy in a given bin, with errors, regardless of whether or not the detection is considered significant. Low significance detections are easily identifiable by their correspondingly large error bars. The minimum flux for a $3\sigma$ detection is $f_{0.5-2\rm keV} \simeq 3 \times 10^{-18}$ erg s$^{-1}$ cm$^{-2}$ ($\log f_{0.5-2\rm keV} \simeq -17.5$).

We plot $U_{\rm n}$, $G$, $\mathscr{R}$ and $I$ magnitude versus X-ray flux (Figure 4). Correlations between magnitude and soft X-ray flux, in the sense that the brightest UV sources are also the brightest X-ray sources, are seen for each filter. Spearman's rank and Pearson's linear correlation tests show each of the relations to be highly significant (e.g. Pearson's linear correlation coefficients were -0.93, -0.93, -0.95, -0.99, all with significance >99 per cent, for $U_{\rm n}$, $G$, $\mathscr{R}$ and $I$ respectively, Table 2). Rest-frame 1–4 keV X-ray emission and rest-frame UV emission are therefore related even before the effects of dust attenuation are applied. The results of the stacking in the six $U_{\rm n}$ bins, which with a rest-frame wavelength of ∼1800 Å at $z\sim1$ corresponds to the wavelength commonly used for UV measures of SFR, are shown in Table 1. Only the weakest bin, $25.25 < U_n \leqslant 27.03$, does not have a significant ($> 3\sigma$) X-ray detection.

The relations between X-ray flux and the colours of the BBGs is less clear. For $U_{\rm n} - G$, a measure of the spectral slope in the far UV, the X-ray signal of the undetected sources is approximately flat for varying colour (Figure 5). With respect to $G - \mathscr{R}$ colour again the X-ray signal is approximately flat, with perhaps some evidence for a slight increase

**Table 1.** Stacking results of undetected BBGs for entire sample and sub-samples based on rest-frame 1800 Å emission. Col.(1): Galaxy sample. Col.(2): Observed-frame energy band. Col.(3): Number of galaxies included in stacking sample, taking into account rejected galaxies as described in §2.5. Col.(4): Mean $\mathscr{R}$ magnitude. Col.(5): Mean redshift. Col.(6): Signal-to-noise ratio $[S/\sqrt{S+B}]$, where S and B are the net source and background counts respectively. Col.(7): X-ray flux per galaxy; 0.5–2 keV for soft band, 2–10 keV for hard band. Col.(8): X-ray luminosity per galaxy in the 2–10 keV band, derived from soft band flux assuming $\Gamma$=2.0 and Galactic $N_H$. 10–50 keV luminosity is given for the hard band, also assuming $\Gamma$=2.0. Col.(9): SFR from 2–10 keV luminosity (Ranalli et al. 2003). Errors are statistical only. Col. (10): Ratio of X-ray derived SFR to UV SFR, uncorrected for attenuation.

| Sample | Band | N | $\langle\mathscr{R}\rangle$ | $\langle z\rangle$ | S/N | $F_X$ ($10^{-18}$ erg cm$^{-2}$ s$^{-1}$) | $L_X$ ($10^{40}$ erg s$^{-1}$) | $\langle SFR\rangle$ ($M_\odot$ yr$^{-1}$) | $SFR_X/SFR_{UV}^{uncor}$ |
|---|---|---|---|---|---|---|---|---|---|
| (1) | (2) | (3) | (4) | (5) | (6) | (7) | (8) | (9) | (10) |
| Undetected BBGs | Soft | 216 | 23.42 | 0.95 | 11.2 | $5.51 \pm 0.49$ | $2.97 \pm 0.26$ | $6.0 \pm 0.6$ | $3.0 \pm 0.4$ |
| Undetected BBGs | Hard | 216 | 23.42 | 0.95 | 3.0 | $8.87 \pm 2.91$ | $7.07 \pm 2.32$ | ... | ... |
| $22.57 < U_n \leqslant 23.72$ | Soft | 34 | 22.50 | 0.91 | 6.7 | $10.21 \pm 1.53$ | $4.81 \pm 0.72$ | $9.6 \pm 1.4$ | $1.8 \pm 0.3$ |
| $23.72 < U_n \leqslant 24.13$ | Soft | 30 | 22.96 | 0.92 | 5.7 | $8.81 \pm 1.44$ | $3.83 \pm 0.68$ | $7.7 \pm 1.4$ | $2.6 \pm 0.5$ |
| $24.13 < U_n \leqslant 24.40$ | Soft | 38 | 23.35 | 0.97 | 5.2 | $6.25 \pm 1.21$ | $3.37 \pm 0.65$ | $6.7 \pm 1.3$ | $2.7 \pm 0.5$ |
| $24.40 < U_n \leqslant 24.71$ | Soft | 40 | 23.63 | 0.97 | 3.1 | $3.25 \pm 1.04$ | $1.75 \pm 0.56$ | $3.5 \pm 1.1$ | $1.8 \pm 0.6$ |
| $24.71 < U_n \leqslant 25.25$ | Soft | 39 | 23.83 | 0.96 | 3.9 | $4.02 \pm 1.03$ | $2.16 \pm 0.56$ | $4.3 \pm 1.1$ | $3.2 \pm 0.8$ |
| $25.25 < U_n \leqslant 27.03$ | Soft | 35 | 24.16 | 0.97 | 2.5 | $2.63 \pm 1.07$ | $1.42 \pm 0.58$ | $2.8 \pm 1.2$ | $4.4 \pm 1.8$ |

**Table 2.** Spearman's rank and linear Pearson's correlation tests. Col.(1): The two quantities being tested. Cols. (2) and (3): Spearman rank correlation coefficient and chance probability. Cols. (4) and (5): Linear Pearson correlation coefficient and chance probability. In each test a coefficient of -1, 0 and +1 indicates a negative correlation, no correlation and a positive correlation, respectively.

| Test pair | Spearman rank Coefficient | Prob. | Linear Pearson Coefficient | Prob. |
|---|---|---|---|---|
| (1) | (2) | (3) | (4) | (5) |
| log $f_x$, $U_n$ | -0.943 | <0.005 | -0.927 | 0.008 |
| log $f_x$, G | -0.886 | 0.019 | -0.934 | 0.006 |
| log $f_x$, $\mathscr{R}$ | -0.943 | <0.005 | -0.953 | <0.005 |
| log $f_x$, I | -1.000 | <0.005 | -0.988 | <0.005 |
| log $f_x$, $(U_n - G)$ | -0.257 | 0.623 | 0.143 | 0.787 |
| log $f_x$, $(G - \mathscr{R})$ | 0.428 | 0.397 | 0.468 | 0.349 |
| log $f_x$, $(\mathscr{R} - I)$ | 0.114 | 0.623 | 0.114 | 0.829 |
| log $L_x$, log $L_{UV}$ | 0.943 | <0.005 | 0.915 | 0.010 |
| $\log(SFR_x/SFR_{UV})$, E(1800Å–2400Å) | 0.486 | 0.329 | 0.855 | 0.030 |
| $\log(SFR_x/SFR_{UV})$, E(2400Å–3400Å) | 0.771 | 0.072 | 0.892 | 0.017 |
| $\log(SFR_x/SFR_{UV})$, E(3400Å–4050Å) | 0.714 | 0.111 | 0.840 | 0.036 |

in X-ray flux with increasing redness. The results for $\mathscr{R} - I$, a measure of the spectral slope near the Balmer break, also show no evidence of a relation with X-ray emission. Binning on colour excess, which removes any redshift dependence in the colours, produced very similar results to those shown in Figure 5: UV colour excess therefore also showed no clear correlation with X-ray flux. Spearman's rank and Pearson's linear correlation tests confirm the absence of a significant correlation between colour and X-ray flux (Table 2).

## 4 DISCUSSION

### 4.1 Stacking signal and SFR estimate

The X-ray emission from the undetected BBGs included in the stacking analysis should not be dominated by AGN as we excluded from the analysis all galaxies that were directly detected, equating to a $L_{2-10\ \mathrm{keV}} \gtrsim 10^{41}$ erg s$^{-1}$ cut-off at $z\sim1$, therefore removing all moderate and luminous AGN. The mean stacking signal is certainly not dominated by a few AGN just below the detection threshold, as is demonstrated by the counts-in-cell distribution shown in Figure 3. The presence of highly obscured AGN can also be ruled out from the observed soft spectrum of the stacking signal. With significant stacked detections in both the soft and hard bands we calculated the mean hardness ratio (HR = (H − S)/(H + S), where H and S are the net hard and soft band counts) of the sample. We find that HR=−0.54±0.11, which is consistent with a $\Gamma \sim 1.8\pm0.3$ unabsorbed power-law spectrum at $z\sim1$. While limited by large errors this result is consistent with the observed spectra of local starburst and star forming galaxies (e.g. Ptak et al. 1999) and is inconsistent with the hard spectrum expected if there was a significant population of obscured AGN within the sample (e.g. the spectrum of the X-ray background). This supports the assumption that the emission from the BBGs is a result of star formation. In saying this we should point out that the presence of low luminosity AGN (LLAGN), with luminosity less than or comparable to the host galaxies themselves, cannot be ruled out. In-

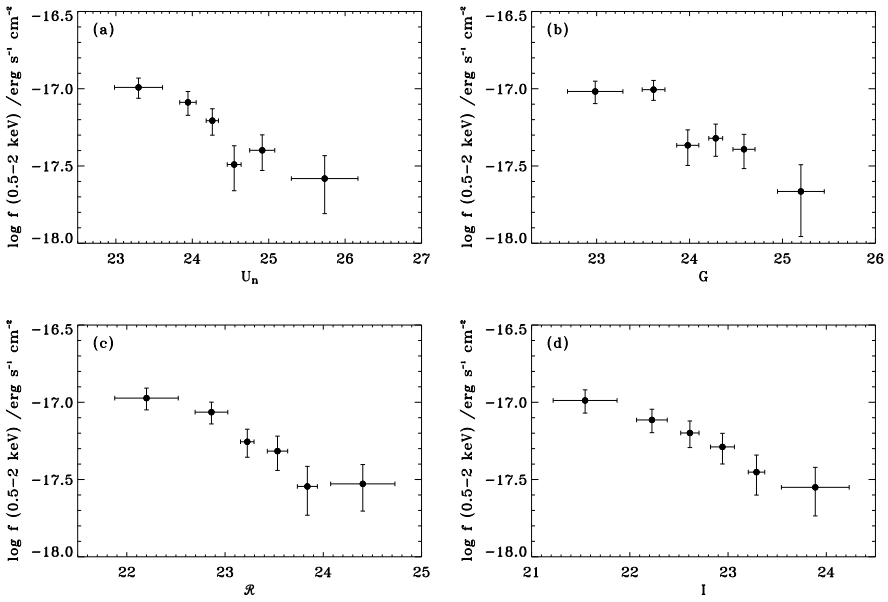


**Figure 4.** X-ray stacking results for undetected BBGs split into subsets according to broad band magnitudes. Correlations of soft X-ray flux with (a) $U_{\rm n}$ magnitude, (b) $G$ magnitude, (c) $\mathscr{R}$ magnitude, and (d) $I$ magnitude are shown. At $z\sim1$ $U_{\rm n}, G, \mathscr{R}$ and $I$ filters correspond to rest-frame ∼1800 Å, ∼2400 Å, ∼3400 Å and ∼4000 Å emission. The $x$-axis errors are standard deviation of values in a given bin, and the $y$-axis error bars are the Poisson errors from stacked soft band counts.

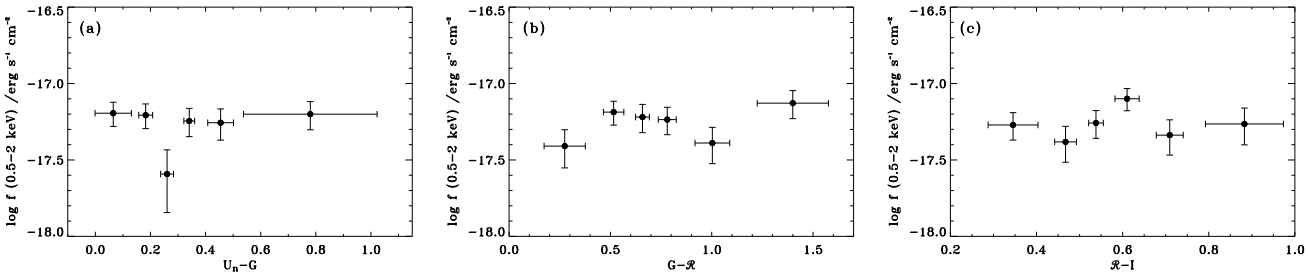


**Figure 5.** X-ray stacking results for undetected BBGs split into subsets according to broad band colours. Correlations of soft X-ray flux with (a) $U_{\rm n}-G$ colour, (b) $G-\mathscr{R}$ colour and (c) $\mathscr{R}-I$ colour are shown. $U_{\rm n}-G$ is a measure of the far-UV slope, $G-\mathscr{R}$ the near-UV slope and $\mathscr{R}-I$ the spectral slope near the Balmer break. The $x$-axis and $y$-axis error bars are as for Figure 4.

deed given the observed incidence of low level nuclear activity in the local Universe (Ho, Filippenko, & Sargent 1997) it is almost certain that there are more as yet undiscovered AGN within the BBG sample. However the contribution of such LLAGN to the mean BBG X-ray luminosity is expected to be small: in a sample of nearby LLAGNs less than one third have X-ray emission that is dominated by a compact nuclear source and the mean 2–10 keV luminosity of the LLAGNs is less than 1 per cent of that of the BBGs (Ho et al. 2001). For the galaxy sample used here we therefore assume that the observed emission is dominated by star formation processes. For such a sample of galaxies the X-ray emission should be proportional to the SFR allowing the X-ray luminosity (normally 2–10 keV) to be used as a SFR measure (N02; Ranalli et al. 2003; Grimm et al. 2003). For situations such as the one here where only the total 2–10 keV luminosity of a galaxy or sample of galaxies is known, and the data render it impossible to resolve the HMXBs either spatially or spectrally, an X-ray–SFR relation with the form of the Ranalli et al. (2003) relation relating the total 2–10 keV emission to SFR should be used. Only in local galaxies, where it is possible to resolve the HMXB population dominating the 2–10 keV flux, can the SFR be derived directly from the total luminosity emitted by HMXBs (e.g. Grimm et al. 2003; Persic et al. 2004).

An additional possible source of contamination is that of emission from LMXBs which reflects the total stellar mass of a system as opposed to the instantaneous SFR. For galaxies with low SFR emission from LMXBs can dominated the flux and the X-rays will cease to measure SFR (Grimm et al. 2003). While we do not attempt to model and separate out the contribution of LMXBs to our measured fluxes we can place approximate upper limits on the expected level of emission from LMXBs in our sample. Studies of the LMXB population in the Milky Way give an estimate of the luminosity from LMXBs per solar mass of stars

(Grimm, Gilfanov, & Sunyaev 2002). Using this result, and assuming that the *mean* stellar mass of the BBGs is no greater than $10^{11}$ $M_\odot$, gives an estimate of the maximum total luminosity from LMXBs per BBG of $5 \times 10^{39}$ erg s$^{-1}$. Under these conditions the contribution of LMXBs to the 2–10 keV luminosity would then be ∼15 per cent for the full sample, rising to ∼30 per cent for the lowest significantly detected bins. We do not therefore expect LMXBs to dominate the emission for this sample of star forming galaxies. *Spitzer* MIPS data, as well as ground based K band imaging, can be used to probe the stellar masses of the BBGs and will allow more stringent estimates of the LMXB contribution to be made. This will be addressed in future work.

Given the expected low contribution from AGN and LMXBs to our detected signal we are confident that the X-ray emission from our sample of undetected BBGs is indeed tracing star formation and we proceed according to this assumption. The observed X-ray fluxes and luminosities which correspond to rest-frame 1–4 keV emission therefore offer us a measure of SFR at $z$∼1 that is relatively unaffected by attenuation by dust, for column densities of $N_H < 10^{22}$ cm$^{-2}$ which corresponds to $A_V \simeq 50$.

Using the empirical relation between the total 2–10 keV luminosity and SFR found by Ranalli et al. (2003), we find that the mean SFR per BBG is $6.0 \pm 0.6$ $M_\odot$ yr$^{-1}$ (Table 1), consistent with that found by N02 for a smaller sample of BBGs using the 1 Ms data. Comparison UV luminosities and estimates of the SFR are calculated from the flux as measured in the $U_n$ band, which at $z$∼1 corresponds to rest frame ∼1800 Å, and the Kennicutt (1998) UV luminosity–SFR relation. These luminosities and SFRs have not been corrected for dust attenuation and should therefore underestimate the SFR compared to X-ray estimates, which better measure the bolometric value. We find $SFR_X/SFR_{UV}^{uncor}$ ∼3 for the full stacking sample, an estimate of the attenuation correction factor for the UV. This attenuation factor is slightly smaller than that found by Reddy & Steidel (2004) for UV selected galaxies at $z$∼2 ($SFR_X/SFR_{UV}^{uncor}$ ∼4.5) and by Nandra et al. (2002) for $z$∼3 LBGs ($SFR_X/SFR_{UV}^{uncor}$ ∼5). This difference is likely due to the mean SFRs of these samples being significantly larger than that considered here: the attenuation factor is similar to the factor of 2.3 found for the SFR<20 $M_\odot$ yr$^{-1}$ subsample of Reddy & Steidel (2004), which has a more similar range in SFRs.

It is important to emphasize that the properties derived for our sample do not necessarily represent the BBGs as a whole. By excluding from our analysis all BBGs with significant direct X-ray detections we will undoubtedly have removed from the sample the galaxies with the highest SFRs, in addition to the AGN dominated sources. With a cut-off luminosity of ∼$10^{41}$ erg s$^{-1}$ this is equivalent to removing all galaxies with SFR $\gtrsim$ 20 $M_\odot$ yr$^{-1}$. The mean SFR, and possibly also UV attenuation factor, of the BBGs as a class is therefore likely to be higher than the values derived here (see §4.2 for further discussion on observed correlations between SFR, attenuation and UV colour).

### 4.2 X-ray–UV correlations and implications

The results of the subset stacking in §3.3 (Figure 4) clearly show that there is a correlation between X-ray flux and UV magnitudes. These correlations, whereby the brightest UV sources are also the brightest X-ray sources, hold over the rest-frame wavelength range 1800–4000 Å. Good, approximately linear, correlations between X-ray luminosity and radio and far infrared (FIR) SFR indicators have been observed before for star forming and starburst galaxies, indicating that the three wavelength regimes are all following the SFR (Ranalli et al. 2003; David et al. 1992). The correlation seen here between X-ray flux and 1800 Å emission also implies that both regimes are tracing the SFR. As discussed above, because rest-frame hard X-rays are relatively unaffected by extinction they should reflect the intrinsic SFR without the need for extinction corrections. On the face of it the observed correlation with X-ray is therefore reassuring in terms of using 1800 Å to measure SFR at high redshift: in general, for UV selected galaxies the sources with the apparent highest SFR also appear to be the brightest in the UV. However given that UV emission is very sensitive to dust attenuation the correlation is a little surprising. Following the generally accepted picture of higher SFR galaxies also being dustier (e.g. Adelberger & Steidel 2000) one might expect the galaxies with large X-ray flux (representing high SFR) to have suppressed UV flux. In Figure 6 we show the relation between X-ray and 1800 Å UV luminosity for the undetected galaxies. Spearman's rank and Pearson's linear correlation tests show a highly significant correlation between log $L_X$ and log $L_{UV}$ (Table 2). The best-fitting power-law is

$$\log(L_{2-10\ \mathrm{keV}}) = (0.62 \pm 0.16)\log(L_{UV}) + 23.01 \pm 4.42 \quad (1)$$

which has an acceptable chi-squared. The best-fit to an exact linear slope

$$\log(L_{2-10\ \mathrm{keV}}) = \log(L_{UV}) + 12.26 \quad (2)$$

is also acceptable, at the 90 per cent level. With no evidence for increasing UV attenuation with increasing SFR, as measured by the X-ray, the observed correlation between X-ray and UV is counterintuitive to general picture of higher SFR galaxies being dustier. The same effect is suggested with the $SFR_X/SFR_{UV}^{uncor}$ ratios in Table 1: for increasing UV flux (and following on from Figures 4 and 6, increasing X-ray flux and SFR) the mean UV attenuation factors actually decrease (though within the errors the results are also con-

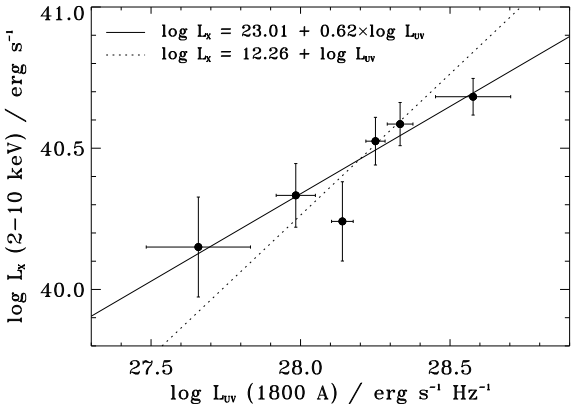


**Figure 6.** 2–10 keV X-ray luminosity vs. 1800 Å UV luminosity, for binning on $U_n$ magnitude. Solid line shows best-fitting power law relation. Dotted line shows best-fitting power law relation with 1-to-1 mapping between X-ray and UV luminosity.

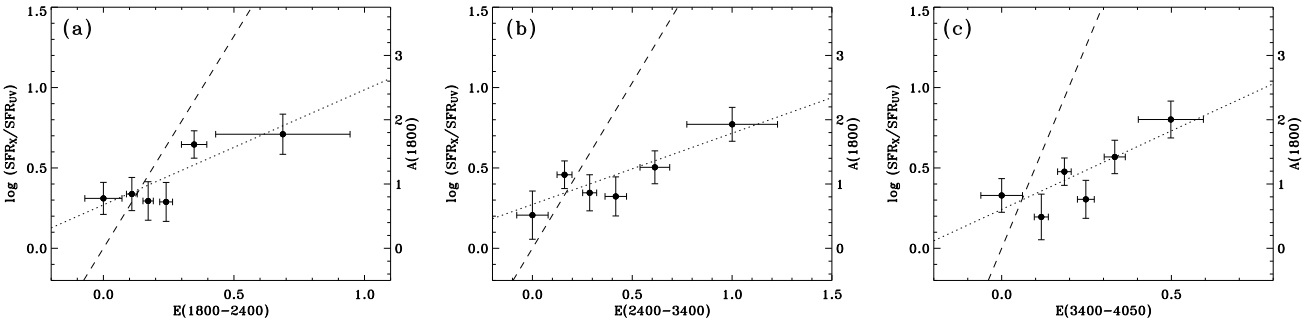


**Figure 7.** Correlations between the ratio of X-ray derived SFR to UV derived SFR (and equivalently $A_{1800}$) and colour excess for undetected BBGs. The UV SFR was calculated from the $U_n$ band and is not corrected for attenuation. The sample was binned according to (a) E(1800Å–2400Å), (b) E(2400Å–3400Å) and (c) E(3400Å–4050Å) colour excess. Dotted lines show best-fitting relations with the form $\log(SFR_X/SFR_{UV}) = a + (b \times \text{colour excess})$. Dashed lines show the Calzetti et al. (2000) attenuation law.

sistent with an approximately constant attenuation factor over the small range in SFRs covered here). These results suggest that UV attenuation may not necessarily be a direct function of SFR over the range of SFRs considered here.

The subset stacking also showed there to be no relation between redness in the UV and X-ray flux (Figure 5) the immediate interpretation of which is that there is no direct correlation between the colour of the UV selected galaxies and their SFRs. Local starbursts exhibit a strong correlation between UV colour and dust absorption, as measured for example by the ratio of far-infrared to UV flux, implying that the starbursts redden as the dust absorption increases and allowing UV attenuation to be estimated purely as a function of UV colour (MHC99). Furthermore the locally derived starburst attention laws appear to hold for high-$z$ UV-selected galaxies such as LBGs (e.g. Seibert et al. 2002; Reddy & Steidel 2004). In order to investigate if such a correlation between colour and attenuation is seen for the $z\sim1$ UV selected galaxies and if the local relations hold we plot the ratio of X-ray to UV derived SFR for subsets binned on colour excess (Figure 7). Since the X-ray SFR estimates should be unaffected by absorption this ratio is a measure of UV attenuation. In Figure 7 we also show the corresponding attenuation coefficient, $A_{1800}$, related to the SFR ratio by $SFR_X/SFR_{UV} = 10^{0.4A_{1800}}$. Correlations between colour excess and attenuation are seen for each of the three bands, with linear correlation tests (Table 2) revealing the strongest correlation to be with E(2400Å–3400Å). For each, we fit a linear function $\log(SFR_X/SFR_{UV}) = a + (b \times \text{colour excess})$, where a and b are constants, which is similar in form to that derived by Calzetti et al. (2000). Each fit yields an acceptable $\chi^2$, with E(2400Å–3400Å) producing the best fit. By binning the data on UV colour excess and calculating the corresponding X-ray and UV SFRs for each bin we find the correlation between UV colour, UV derived SFR and X-ray derived SFR to be

$$SFR_X = (1.87^{+0.41}_{-0.61}) \times 10^{(0.44^{+0.20}_{-0.25})E(2400-3400)} SFR_{UV}, \quad (3)$$

where errors are for $\Delta\chi^2 = 2.7$, or 90 per cent confidence, for one interesting parameter. For the SFRs covered in our sample, and over a range in colour excess of $\Delta E \simeq 1$, we find that the UV attenuation ranges from 0.5 to 2.0 magnitudes at 1800 Å, corresponding to relatively modest UV correction factors of $\sim 1.5 - 6.5$. The observed colour–attenuation results, while certainly limited by the number of fitting points and large errors, show clearly that UV colour is correlated with dust attenuation for UV selected galaxies at $z\sim1$. This key result allows a single UV colour to be used to estimate UV attenuation corrections and attenuation corrected SFRs, as shown above in Equation 3.

The attenuation coefficients, $A_{1800}$, and corresponding values of $\log(SFR_X/SFR_{UV})$ predicted by the reddening curve and attenuation law of Calzetti et al. (2000) are also shown in Figure 7. For a given reddening curve, the implied relationship between attenuation, $A_{1800}$, and colour excess, E, is nearly independent of the assumed underlying galaxy template. The Calzetti lines in Figure 7 are appropriate for galaxy spectral types Im, Sc, and Sb which span the expected range for BBGs. While the normalisation of our data points with respect to absolute values of colour excess was approximate, and therefore the relative normalisation between our data and the Calzetti prediction is also approximate, the main conclusion is clearly visible: the Calzetti law over predicts the attenuation corrections compared to the observed values. Between E(1800Å–2400Å)=0 and E(1800Å–2400Å)=1 approximately 7 magnitudes of extinction are predicted at 1800 Å, compared to the observed difference of ∼2 magnitudes – an over prediction of the range in UV luminosity and UV SFR correction factors of ∼100. For a typical galaxy in our sample with E(1800Å–2400Å)=0.25, the Calzetti law predicts $A_{1800}$ =1.7 compared to the observed $A_{1800}$ =1.1 – an over prediction in the UV SFR correction factor of 1.6. For E(1800Å–2400Å), E(2400Å–3400Å) and E(3400Å–4050Å) the probability that the data are derived from the Calzetti model is < 0.01 per cent, regardless of the exact position of the Calzetti slope relative to the data points. The failure of the Calzetti attenuation law at predicting the attenuation of the galaxies in our sample is most likely a result of the inherent differences in the sample of galaxies used here and those from which the attenuation laws were calculated. The attenuation laws were derived for local starburst galaxies for which the UV colours are predominantly affected by dust content and obscuration. BBG selection on the other hand identifies Sb- and Sc-type star forming galaxies as well as starbursts (Adelberger et al. 2004) and therefore includes galaxies with more quiescent

star formation, and a range of star formation histories and stellar population ages which affect the UV colours as much as the dust content. Such samples of galaxies clearly do not follow the starburst attenuation laws.

## 5 SUMMARY

With the 2 Ms observation of the HDF-N region we have examined the X-ray properties of a large sample of UV-selected, star forming galaxies with $0.74 < z < 1.32$. In this paper we dealt exclusively with the 216 galaxies in the sample that are not directly detected in X-ray and whose emission should be predominately due to star formation processes (analysis of the detected BBGs will be presented in an upcoming paper, Laird et al., in preparation). Here we summarise our main results:

(i) Stacking the soft band flux from the undetected BBGs resulted in a highly significant, $14.9\sigma$ detection. The detected signal corresponds to a mean flux per galaxy of $5.51 \pm 0.49 \times 10^{-18}$ erg s$^{-1}$ cm$^{-2}$ (0.5–2 keV) and a mean luminosity of $L_{2-10keV} = 2.97 \pm 0.26 \times 10^{40}$ erg s$^{-1}$.

(ii) Stacking the hard band flux also resulted in a significant detection of low level emission. We find a mean 2-10 keV flux per undetected BBG of $8.87 \pm 2.91 \times 10^{-18}$ erg s$^{-1}$ cm$^{-2}$.

(iii) The hardness ratio of the sample, HR$= -0.54 \pm 0.11$, is consistent with a $\Gamma \sim 1.8 \pm 0.3$ unabsorbed power-law spectrum. This is consistent with the integrated spectrum from HMXBs and supports the general interpretation that the detected emission is due to normal star formation processes.

(iv) The mean X-ray derived SFR of the sample of undetected BBGs is $6.0 \pm 0.6$ M$_\odot$ yr$^{-1}$. The ratio of X-ray derived SFR to UV derived SFR, an indication of the average UV attenuation factor, is 3.

(v) Splitting the sample into subsets based on observed-frame optical magnitudes and colours and stacking the X-ray flux in each bin produced significant detections, allowing correlations between X-ray and UV emission to be examined. We find clear correlations between X-ray flux and rest-frame UV flux (over the range $\sim$1800–4000 Å) such that galaxies that are brighter in the UV are also brighter in X-ray. There is no evidence for a correlation between UV colour or UV colour excess and X-ray flux.

(vi) Correlations between colour excess and the ratio of X-ray-to-UV SFRs (which measures UV attenuation) are seen, whereby the ratio of X-ray-to-UV increases with UV redness. Using the data we derive a relation for estimating UV attenuation corrections from UV colour excess.

(vii) The observed relation between colour excess and attenuation is found to be inconsistent with the Calzetti et al. (2000) and MHC99 extinction curve which over predict the range in attenuation corrections for the galaxies in this sample by a factor of $\sim$100.

## ACKNOWLEDGMENTS

We thank the referee for helpful comments that improved the manuscript and the *Chandra* X-ray Center for assistance with some analysis and software issues. D. Rosa-González is thanked for many useful discussions. ESL acknowledges the support of a PPARC Studentship and a University of London Valerie Myerscough Prize.

## REFERENCES

Adelberger K. L., Steidel C. C., 2000, ApJ, 544, 2
Adelberger K. L., Steidel C. C., Shapley A. E., Hunt M. P., Erb D. K., Reddy N. A., Pettini M., 2004, ApJ, 607, 266
Alexander D. M. et al. 2003, AJ, 126, 539
Bell E. F., 2002, ApJ, 577, 150
Brandt W. N., Hornschemeier A. E., Schneider D. P., Alexander D. M., Bauer F. E., Garmire G. P., Vignali C., 2001, ApJL, 558, L5
Calzetti D., Kinney A. L., Storchi-Bergmann T., 1994, ApJ, 429, 582
Calzetti D., Armus L., Bohlin R. C., Kinney A. L., Koornneef J., Storchi-Bergmann T., 2000, ApJ, 533, 682
David L. P., Jones C., Forman W., 1992, ApJ, 388, 82
Fabbiano G., 1989, ARA&A, 27, 87
Giavalisco M., 2002, ARA&A, 40, 579
Grimm H.-J., Gilfanov M., Sunyaev R., 2002, A&A, 391, 923
Grimm H.-J., Gilfanov M., Sunyaev R., 2003, MNRAS, 339, 793
Ho L. C., Filippenko A. V., Sargent W. L. W., 1997, ApJ, 487, 568
Ho L. C., et al., 2001, ApJ, 549, L5
Hornschemeier A. E., et al., 2001, ApJ, 554, 742
Hughes D. H., et al., 1998, Nat, 394, 241
Kennicutt R. C., 1998, ARA&A, 36, 189
Lehmer B. D., et al., 2005, AJ, 129, 1
Lilly S. J., Le Fevre O., Hammer F., Crampton D., 1996, ApJ, 460, L1
Madau P., Ferguson H. C., Dickinson M. E., Giavalisco M., Steidel C. C., Fruchter A., 1996, MNRAS, 283, 1388
Marshall H. L., Tennant A., Grant C. E., Hitchcock A. P., O'Dell S. L., Plucinsky P. P., 2004, SPIE, 5165, 497
Meurer G. R., Heckman T. M., Calzetti D., 1999, ApJ, 521, 64
Nandra K., Mushotzky R. F., Arnaud K., Steidel C. C., Adelberger K. L., Gardner J. P., Teplitz H. I., Windhorst R. A., 2002, ApJ, 576, 625
Nandra K., et al., 2005, MNRAS, 356, 568
Persic M., Rephaeli Y., Braito V., Cappi M., Della Ceca R., Franceschini A., Gruber D. E., 2004, A&A, 419, 849
Ptak A., Serlemitsos P., Yaqoob T., Mushotzky R., 1999, ApJS, 120, 179
Ranalli P., Comastri A., Setti G., 2003, A&A, 399, 39
Reddy N. A., Steidel C. C., 2004, ApJ, 603, L13
Seibert M., Heckman T. M., Meurer G. R., 2002, AJ, 124, 46
Stark A. A., Gammie C. F., Wilson R. W., Bally J., Linke R. A., Heiles C., Hurwitz M., 1992, ApJS, 79, 77
Steidel C. C., Giavalisco M., Pettini M., Dickinson M., Adelberger K. L., 1996, ApJ, 462, L17
Steidel C. C., Adelberger K. L., Giavalisco M., Dickinson M., Pettini M., 1999, ApJ, 519, 1
Steidel C. C., Adelberger K. L., Shapley A. E., Pettini M., Dickinson M., Giavalisco M., 2003, ApJ, 592, 728
Steidel C. C., Shapley A. E., Pettini M., Adelberger K. L., Erb D. K., Reddy N. A., Hunt M. P., 2004, ApJ, 604, 534

Wirth G. D., et al., 2004, AJ, 127, 3121